Methanol Distribution and Electroosmotic Drag in Hydrated Poly(perfluorosulfonic) Acid Membrane

ARTICLE *in* THE JOURNAL OF PHYSICAL CHEMISTRY B · JANUARY 2009

Impact Factor: 3.3 · DOI: 10.1021/jp8066469 · Source: PubMed

5 AUTHORS, INCLUDING:

Liuming Yan
Shanghai University
66 PUBLICATIONS **832** CITATIONS
SEE PROFILE

Suhua Zhu
Changshu Institute of Technology
6 PUBLICATIONS **79** CITATIONS
SEE PROFILE

Wencong Lu
Shanghai University
56 PUBLICATIONS **694** CITATIONS
SEE PROFILE

Methanol Distribution and Electroosmotic Drag in Hydrated Poly(perfluorosulfonic) Acid Membrane

Xiaobo Ji,[†,‡] Liuming Yan,*[,‡] Suhua Zhu,[†,‡] Liangmiao Zhang,[†,‡] and Wencong Lu[‡]

School of Material Science and Engineering, Department of Chemistry, College of Sciences, Shanghai University, 99 Shangda Road, Shanghai 200444, China

Received: July 26, 2008; Revised Manuscript Received: October 11, 2008

The methanol distribution and electroosmotic drag in hydrated poly(perfluorosulfonic) acid electrolyte membrane are studied using molecular dynamics simulations under various electric fields applied. The results indicate that the methanol molecules are preferentially distributed near the hydrophobic PFSA backbones with their methyl groups in contact with the fluorine atoms and their hydroxyl groups pointing to the hydrophilic subphase. As the hydroxyl groups of methanol forming hydrogen bonds, hydroxyl groups are more likely to accept hydrogen atoms than to donate hydrogen atoms. The calculated methanol diffusion coefficient is in good correspondence with experimental values, and the electroosmotic drag coefficient for methanol is much smaller than that of water molecules.

1. Introduction

Direct methanol fuel cells (DMFCs) have found potential applications in fields ranging from small portable consumer electronics[1,2] to vehicles[3] for their high energy conversion efficiency, high energy density, simplicity of operation, and so forth. Now DMFCs are considered to be competitive alternative for the hydrogen proton exchange membrane fuel cells (PEMFCs), which are potential energy conversion devices for the next generation vehicles.[4,5] Compared to the complex, inefficiency, and costly storage and delivery systems for hydrogen, methanol could be efficiently stored and delivered as a liquid. Furthermore, the existing storage and delivery infrastructures developed for petroleum-based liquid fuels can be readily converted to the storage and delivery of liquid methanol with low expenses. Despite these advantages, technical barriers still need to be overcome for their large scale commercialization of DMFCs.[6] One of such technical barriers is the methanol crossover, or the direct transport of methanol from anode to cathode via the proton exchange membrane. Methanol crossover will not only lead to reduced energy conversion efficiency because of the direct chemical oxidation of methanol in the cathodic half-cell that hence drastically degrades fuel cell performance but also cause fuel cell operational failures.

The methanol crossover has been extensively investigated by the experimental measurement of the CO_2 concentration in the cathodic exhaust gas, by the cyclic voltammetry measurement, or by the direct detection of methanol concentration in the membrane using techniques such as NMR. By measuring the CO_2 concentration in cathodic exhaust gas using gas chromatography, Schaffer et al. found that the combined electroosmotic drag coefficient, including both contributions from water and methanol, increases with fuel cell operation temperature, current density, and methanol concentration.[7,8] Furthermore, an inverse relationship was found to exist between the cathode humidification temperature and methanol crossover.[6] By application of the cyclic voltammetry measurement, Ren et al. found that the methanol transport increases in temperature range from 30 to 100 °C in a swollen NAFION membrane with an activation energy of 4.8 kcal/mol,[9] Kallio and co-workers observed lowered permeability in radiation-grafted membranes compared to the native NAFION 115 membrane,[10] and Ramya et al. observed reduced methanol permeability in the NAFION 117 or NAFION 1135 membranes after these membranes are heated at an elevated temperature between their glass transition temperatures and degradation temperatures.[11] By applying NMR to the direct detection of methanol concentration, Aricò et al. determined the self-diffusion coefficient of methanol in DMFC over a wide range of temperature,[12] and Paik et al. detected methanol concentration in NAFION 117 membrane during fuel cell operation.[5] Despite its popularity, the determination of methanol crossover by measurement of CO_2 concentration in the cathodic exhaust gas is suspicious, because it is based on the hypotheses that methanol crossover the proton exchange membrane is completely oxidized to CO_2, and that CO_2 diffusion from anode to cathode is negligible. The other common disadvantage of these experimental methods is that one cannot distinguish the many different transport flows caused by different mechanisms that exist simultaneously. To our knowledge, methanol crossover coefficient that is induced exclusively by the electroosmotic drag in hydrated poly(perfluorosulfonic) acid by aqueous methanol solution is still not reported in the literature.

For the further elucidation of water and methanol transport in ionomer membranes, a number of physical models have also been developed as beneficial complement to the experimental researches.[13,14] For example, Cruickshank and Scott presented a simple methanol transport model based on the Nernst−Planck equation and successfully explained the voltage-current response to the methanol crossover under different oxygen pressure and methanol concentration.[13,15] Jeng developed a mathematical model to describe mass transport in the anode compartment and in the proton exchange membrane and the effect of kinetic and ohmic resistance of the anodic catalyst in the anode of a DMFC and showed that the methanol crossover increases with methanol concentration even under low current density.[14] Schultz et al. modeled the mass transport inside the polymer electrolyte

* To whom correspondence should be addressed. E-mail: liuming.yan@shu.edu.cn.
† School of Material Science and Engineering.
‡ Department of Chemistry, College of Sciences.

10.1021/jp8066469 CCC: $40.75
Published on Web 11/14/2008

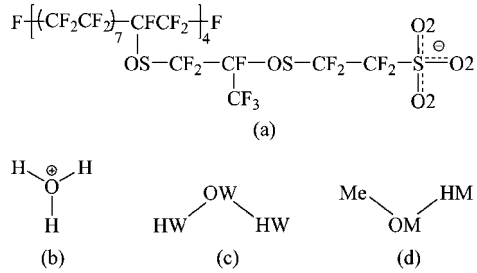

Figure 1. Molecular illustrations and site names of the PFSA oligomer hydrated by the aqueous solution of methanol in the simulation system: (a) PFSA oligomer; (b) hydronium; (c) water; and (d) methanol.

membrane by combination of the generalized Maxwell−Stefan equations and the Flory−Huggins activity model and obtained good approximations compared to the experimental measurement.[16] These theoretical models have provided some valuable qualitative insights; however, each of them applies in one case but fails in the other cases, and the complete representation of the transport process remains great challenge.

In this work, we will extend our previous molecular dynamics simulation method developed for the evaluation of water electroosmosis in hydrated perfluorosulfonic acid oligomers to the investigation of methanol diffusion and electroosmosis, as well as the methanol distribution and the membrane microstructure.[17] The hydrogen bonding characteristics of methanol with sulfonate anion groups, hydronium cations, and water molecules will be investigated by employing both molecular dynamics simulations and first principle calculations. These characteristics are fundamental important in the understanding of methanol crossover.

2. The Molecular Models and the Calculation Methods

2.1. The Molecular Models. The simulation system is composed of 12 perfluorosulfonic acid oligomers (PFSA), which are modeled by oligomers each consisting of a 64 carbon long poly(tetrafluoroethylene) backbone and four pendant side chains terminated by sulfonic acid groups (Figure 1a). All the sulfonic acid groups are supposed to be ionized leaving a negatively charged sulfonate anion terminating group $-SO_3^-$, and 48 hydronium cations are added as counterions to keep the electric neutrality of the system. In addition, 816 water molecules and 96 methanol molecules, corresponding to an aqueous solution of methanol at approximately 5 mol/dm^3, are also included in the simulation system (the hydration degree of the hydrated perfluorosulfonic electrolyte is 18).

The force field employed for the PFSA is based on the modified all-atom OPLS force field.[18] All the force field parameters are described in elsewhere.[19] The united-atom force field model is used for methanol.[20] The rigid TIP3P models are applied for hydroniums and water molecules.[21,22] For discussion convenience, site names are defined as the following and as in Figure 1: O2, OS, O, OW, and OM for oxygen of sulfonate anion group $-SO_3^-$, ether oxygen, oxygen of hydronium cation, oxygen of water, and oxygen of methanol, respectively; H, HW, and HM for hydrogen of hydronium cation, hydrogen of water, and hydrogen of the methanol hydroxyl; and C and F for carbon and fluorine in the PFSA oligomer. In addition, the methyl group of methanol, which is modeled by a united-atom, is represented by the site name Me.

The initial configuration is constructed using a random inserting scheme. The coordinates of all the atoms of the PFSA oligomers are set first, and then the water molecules, the hydronium cations, and the methanol molecules are randomly inserted into the simulation cell one by one. This initial configuration corresponds to a loose structure with a density of about 0.5 g/cm^3. During the initial simulation, this loose configuration is gradually squeezed and reaches to its equilibrated density 1.61 g/cm^3. The calculated density of this system is 1.57∼1.61 g/cm^3 by assuming of equal volume mixing and if the density of dry PFSA oligomers, water, and methanol are 2.0∼2.1, 1.0, and 0.79 g/cm^3, respectively. The concentration gradient is an important factor that causes the methanol diffusion in real world DMFC; however, concentration gradient is not implemented in our simulations since it is difficult to maintain any significant concentration gradient in the simulation cell with limited volume.

2.2. The Simulation Details. Molecular dynamics simulations are carried out in the NPT ensemble by application of the Nosé−Hoover thermostat[23] as implemented in DL_POLY program.[24] Periodic boundary conditions are applied to exclude the interfacial effects of the limited system. Lennard-Jones interactions are cut off at 8.5 Å, and the Ewald summation algorithm is applied to the calculation of electrostatic potential energy in account for long-range Coulombic interactions. In the simulations, the Verlet leapfrog integration algorithm is employed with a time step of 1.0 fs, and the relaxation times for the thermostat and barostat are set to 0.1 ps.[25,26]

During the simulation, the initial configuration is equilibrated at 300 K and 1 atm for 1 000 000 time steps. Then, an electric field (at 0, 1, 2, or 5 V/μm, respectively) is turned on and another 10 000 time steps are run. Finally, 90 000 time steps are carried out, and snapshots of the coordinates and velocities of all atoms are recorded every 10 time steps in a history file. This recorded history file is used to generate various properties including the structural characteristics, velocity distribution functions, and electroosmotic drag coefficient.

3. Calculation Results

3.1. Structural Characteristics of PFSA Hydrated by Aqueous Methanol Solution. ***3.1.1. The Microstructure.*** Several structural models have been applied to the understanding of the microstructure and molecular distribution in PFSA.[27] The cluster-channel model based on the wide- and small-angle X-ray scattering studies (WAXS and SAXS) is the most widely accepted description for the microstructure of PFSA in which the hydrated PFSA is segregated into hydrophobic and hydrophilic subphases, and the hydrophilic side chains aggregate at the interface of the hydrophobic and hydrophilic subphases.[28] In Figure 2, it shows one snapshot of the PFSA hydrated by aqueous methanol solution from our MD simulation. Despite the differences between pure solvent of water and mixed solvent of water and methanol, the microstructure of PFSA hydrated by mixed solvent is similar to that hydrated by pure water as reported in literature.[29] The hydrated PFSA by mixed solvent also forms a reversed micelle structure of water-in-oil; the PFSA oligomer backbones aggregate and fold to form a hydrophobic subphase; the water, methanol, and hydronium gather together to form a hydrophilic subphase wrapped in the oligomer backbones. Furthermore, the hydrophilic side chains permeate into the hydrophilic subphase forming the hydrophobic/hydrophilic interface stabilizing the water-in-oil structure. From Figure 2, it could also be seen that the methanol molecules mainly distribute at the interface of the hydrophobic and hydrophilic subphases (which will be detailed in Section 3.1.3).

3.1.2. Hydrogen Bond Network. The hydrogen bond network plays an important role in the extraordinary high proton mobility of aqueous methanol solution.[30] The knowledge for such

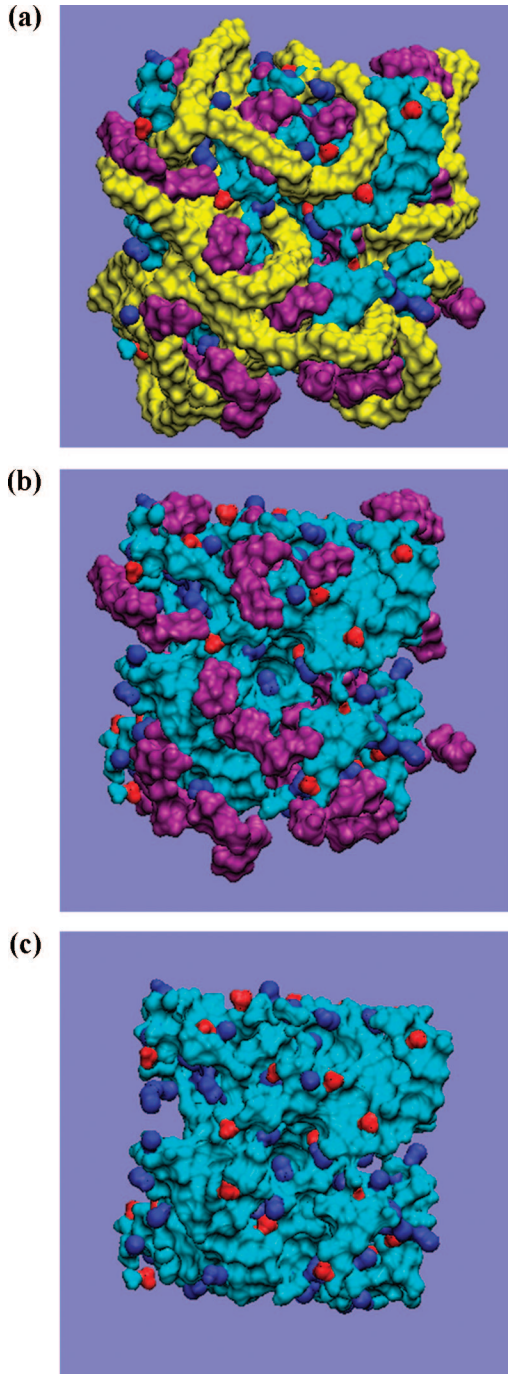

Figure 2. Snapshot of the PFSA hydrated with aqueous solution of methanol from MD simulation, which shows the molecular profile (contour) of the simulation cell: (a) all the molecules are shown, (b) the PFSA backbones are not shown, and (c) the PFSA oligomers are not shown. Molecular moieties are color coded: yellow for the PFSA backbones; purple for the PFSA side-chains; cyan for water molecules; red for hydronium cations; and blue for methanol molecules. In order to have a good view of the molecules, the molecules that span between two periodic simulation cells have been adjusted to be shown contiguously by applying the periodic boundary conditions. Simulation cell size: 42.47 × 42.47 × 42.47 Å.

network is essential to the understanding of many chemically and biologically important processes,[31,32] as well as of many transport processes in the swollen PFSA.[27,33,34] Similar to a water molecule, a methanol molecule in aqueous solution can form hydrogen bonds not only by donating its hydroxyl hydrogen atom, but also by accepting hydroxyl hydrogen from other methanol molecules or water molecules. The difference between

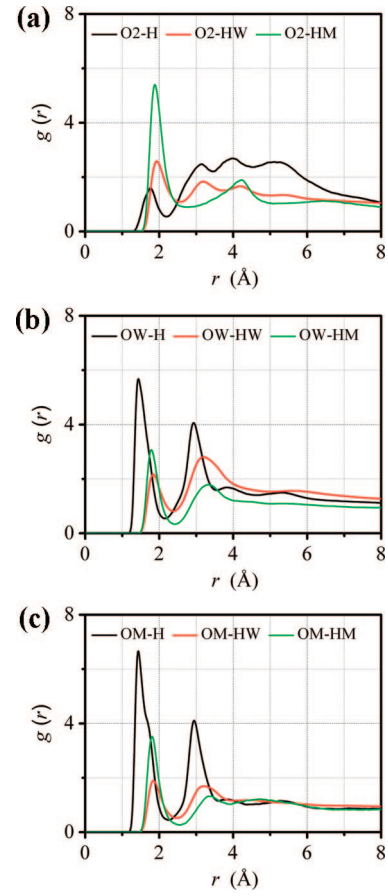

Figure 3. Radial distribution functions that are related to the hydrogen bond network in hydrated PFSA. (a) O2 (sulfonate anion group) - hydrogen; (b) OW (water) - hydrogen; (c) OM (methanol) - hydrogen.

TABLE 1: The First Peak Position (R_p) and Height (h_p), the Valley Position (R_v), and Coordination Number (CN) for RDFs That Are Related to the Hydrogen Bond Network, Where CN′ is the Adjusted Coordination Number Supposing That Hydronium, Water, and Methanol Are the Same Concentration in the Simulation Cell

site pair	R_p (Å)	h_p	R_v (Å)	CN	CN′
O2-H	1.775	1.613	2.175	0.06	1.00
O2-HW	1.925	2.613	2.575	1.86	2.74
O2-HM	1.875	5.494	2.775	0.19	4.75
OW-H	1.425	5.833	2.175	0.15	1.45
OW-HW	1.825	2.192	2.375	1.17	1.00
OW-HM	1.825	3.007	2.425	0.07	1.02
OM-H	1.425	6.907	2.275	0.18	1.94
OM-HW	1.775	1.761	2.475	1.05	1.00
OM-HM	1.825	3.564	2.575	0.08	1.30

the hydrogen bonding behavior of a methanol molecule and a water molecule is that a water molecule can simultaneously donate one or two hydroxyl hydrogen atom (theoretically); however, a methanol molecule can only donate one hydroxyl hydrogen atom. To the better understanding of the hydrogen bond network in the hydrated PFSA by aqueous methanol solution, some of the radial distribution functions (RDFs) related to the hydrogen bonds are reported in Figure 3, and the important characteristics are summarized in table 1.

All the first peaks for $g_{O2\text{-}H}(r)$, $g_{O2\text{-}HW}(r)$, and $g_{O2\text{-}HM}(r)$, located at 1.775, 1.925, and 1.875 Å, respectively, are in the range of a usual hydrogen bond (Figure 3a). According to their corresponding peak heights of 1.613, 2.613, and 5.494, hydrogen

bonds formed between the O2 and methanol are the strongest, while those between the O2 and hydronium are the weakest. It is interesting that the hydrogen bonds between O2 and hydronium are the weakest despite the strong Coulombic attraction between a hydronium hydrogen and a sulfonate anion oxygen. This phenomenon has been attributed to the introduction of water (or methanol) molecules that pull hydronium cations away from the first coordination shell of the sulfonate anion and into the second shell with higher second peak.[35,36] Although the first coordination number of O2 shows that there are more water molecules in its first coordination shell since each O2 accepts 0.06, 1.86, and 0.19 hydrogen atoms on average from hydronium cations, water molecules, and methanol molecules (table 1), the methanol molecules are actually the most preferred molecules in its first coordination shell. Considering that there are 48, 816, and 96 hydronium cations, water molecules, and methanol molecules in the simulation cell, respectively, the probability to find a hydronium cation, water molecule, or methanol molecule will be adjusted to 1.00/2.74/4.75 (CN′ in Table 1) if the concentration of these moieties are the same. Therefore, the sulfonate anion groups are more likely to attract the neutral methanol molecules by forming a hydrogen bond.

The first sharp peaks of $g_{OW\text{-}H}(r)$, $g_{OW\text{-}HM}(r)$, and $g_{OW\text{-}HW}(r)$ (Figure 3b) reveal that the local structure of a water molecule is highly ordered by forming a hydrogen bond between the water oxygen OW and hydronium cation, methanol molecule, or other water molecule. The strongest hydrogen bond forms between a water oxygen and a hydronium hydrogen with an O···H distance of 1.425 Å owing to the strong attraction between a positively charged hydronium and negatively charged oxygen OW of water. Also, the hydrogen bond between a water molecule and a methanol molecule is stronger than that between two water molecules.[37] From the adjusted coordination number of CN′ in Table 1, it could be found that the water molecule favors hydronium cations most in its first coordination shell. From the second sharp peaks of $g_{OW\text{-}H}(r)$, it could be deduced that the second coordination shell of water is also highly ordered, and a hydrogen bond network exists.[38,39] From the fact that the second peak of $g_{OW\text{-}HW}(r)$ at 3.175 Å is broader and higher than the first peak, it could be concluded that the second coordination shell of water molecule is also filled with the hydrogen bonds, which is consistent with other calculations[22] and experimental studies.[40] In comparison to the $g_{OW\text{-}HW}(r)$, the second peak of $g_{OW\text{-}HM}(r)$ also exists but appears to be lower, indicating that the second coordination shell of water molecules also include the methanol molecules to a certain extent.

The similarity between RDFs related to methanol oxygen and RDFs related to water oxygen (Figure 3b,c) reveals a fact that the hydrogen bonding characteristics of methanol are similar with those of water. From the first peak height of $g_{OM\text{-}H}(r)$, it could be deduced that the strongest hydrogen bond formed between a methanol and a hydronium cation; as a result, methanol is likely to transport accompanying hydronium under an applied electric field. Since the second peaks for $g_{OM\text{-}HW}(r)$ and $g_{OM\text{-}HM}(r)$ are not as significant as those of $g_{OW\text{-}HW}(r)$ and $g_{OW\text{-}HM}(r)$, the second coordination shell of methanol is relatively loose compared to that of water. From the adjusted coordination number, it is also deduced that a methanol molecule is more likely to form a hydrogen bond with the hydronium cation or other methanol molecule than with the water molecule.

These results confirm a continuous hydrogen bond network instead of small hydrogen bond clusters formed by sulfonate anion groups, water molecules, hydronium cations, and methanol molecules, where methanol molecules and water molecules act both as hydrogen donors and hydrogen acceptors, while the sulfonate anion groups (or hydronium cations) only serve as hydrogen acceptors (or hydrogen donors). Among all the hydrogen bonds, the hydrogen bond between methanol and hydronium is the strongest and that between water and hydronium is the second strongest. A continuous hydrogen bond network can facilitate the proton transport; however, this network will also promote the methanol crossover and water electroosmosis. In Figure 4, the hydrogen bond network is visualized by a slice of the simulation cell along the *x*-direction with hydrogen bonds clearly observable.

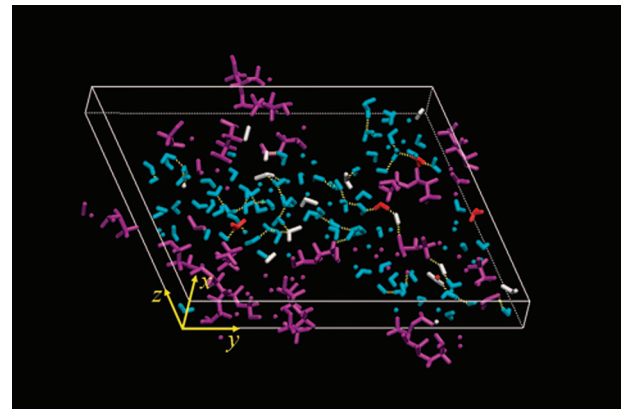

Figure 4. Hydrogen bond network formed in the simulated PFSA oligomers hydrated by aqueous methanol solution (only a slice of the simulation cell is shown). Color codes: purple for the PFSA oligomer; cyan for water; red for hydronium; white for methanol; and yellow dotted lines for hydrogen bonds.

3.1.3. Distribution of Methanol Molecules in the Hydrated PFSA System. Although the hydrophobic methyl group is rather short, methanol still shows biphilic characteristics with its hydroxyl group showing hydrophilicity and interacting strongly with water by forming hydrogen bond network, and its methyl group showing hydrophobicity and interacting strongly with hydrophobic PFSA backbone by van der Waals interactions.[29] As a result, methanol crossover depends not only on the interaction between methanol and water (or hydronium) in hydrophilic subphase but also on the interaction between the methanol and PFSA oligomer in hydrophobic subphase. In this section, the methanol distribution will be discussed in terms of RDFs, as well as in terms of nearest distance distribution in the hydrated PFSA membrane. In Figure 5, the radial distribution functions for methanol-F (or OS), water-F (or OS), and hydronium-F (or OS) are shown, where F (or OS) represents the hydrophobic backbone (or hydrophilic sidechain). For comparison, the RDFs for water molecules and hydronium cations are also shown. From these figures, it could be seen that only the RDFs for methanol show significant peaks at 3.575 Å for $g_{F-Me}(r)$ and at 5.575 Å for $g_{OS-Me}(r)$, suggesting that the methanol not only favorably distributes in the hydrophilic subphase but also in the surroundings of the hydrophobic backbones. On the other hand, the water and hydronium are excluded from the PFSA oligomers.

Although these RDFs do reflect the local distribution of the methanol molecules, water molecules, and hydronium cations near the PFSA oligomers, it is still impossible to evaluate the percentage of molecules (or cations) that are in directly contact (or not) with the PFSA oligomers. In this paragraph, we are going to introduce the nearest distance distribution function, which directly reflects the percentage of molecules which are distributed at certain distance to any of the PFSA oligomers. The calculation process is schematically illustrated in Figure 6.

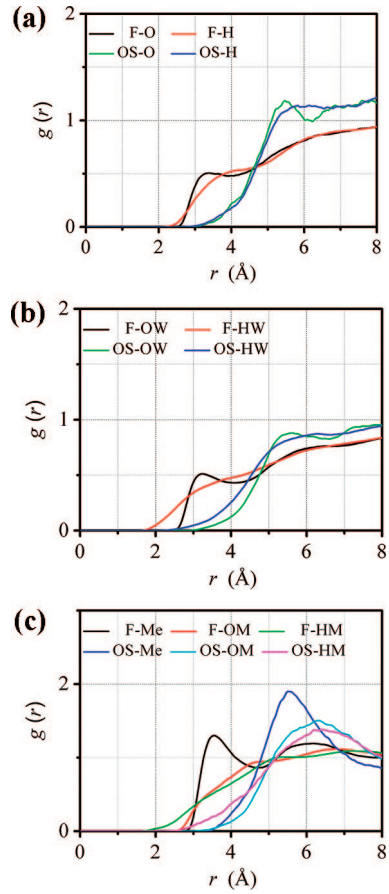

Figure 5. Radial distribution functions for the hydrated PFSA system (a) hydronium−F (or OS); (b) water−F (or OS); (c) methanol−F (or OS).

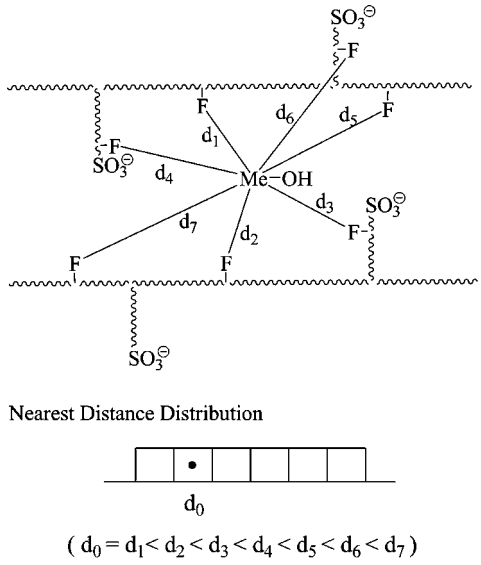

Figure 6. Schematic illustration of the nearest distance distribution function of methyl Me to the fluorine atoms. The waves denote the PFSA oligomers and F's denote fluorine atoms. The nearest distance of a methyl Me to the fluorine atoms, d_0, is found by calculation of all the distances between Me and fluorine atoms, d_i. One difference between the nearest distance distribution function and RDF is that we will count each occurrence of the distance d_i in the histogram of RDF, but only the nearest occurrence d_0 in the nearest distance distribution function histogram.

For any of the recorded snapshot, we first calculate the distances of a methyl Me to all the fluorine atoms F in the system. And then, the nearest distance between Me and F is found. By repeating this process for all the methyl groups, we can find all the nearest distance of any methyl to the fluorine atoms. Finally, the nearest distance distribution function of methyl to F is calculated by averaging over the many snapshots that are recorded during the molecular dynamics simulation.

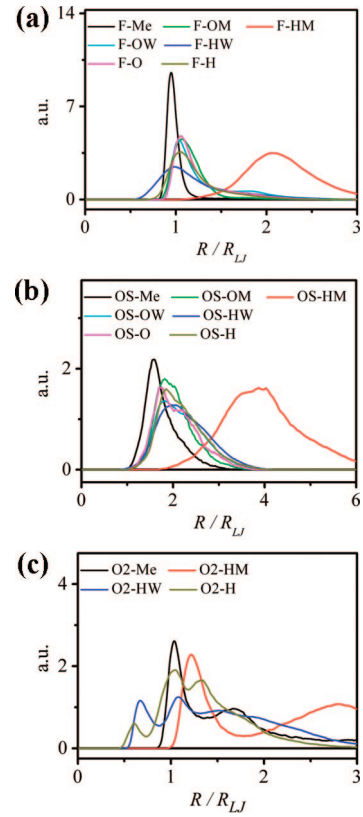

Figure 7. Nearest distance distribution functions for the hydrated PFSA membrane: (a) fluorine−methanol (water or hydronium); (b) ether oxygen−methanol (water or hydronium); and (c) O2−methanol (water or hydronium). R_{LJ} is summation of the Lennard-Jones collision parameters of the two corresponding atoms (or sites).

Figure 7 shows some of the nearest distance distribution functions that reflect the distribution of methanol molecules, water molecules, and hydronium cations near the PFSA oligomer backbone (F), ether oxygen (OS), or sulfonate anion group (O2). From the sharp peak (located at 0.955 R_{LJ}) of the nearest distance distribution function for methyl (Me) and fluorine atom (F) and the broad peak for HM-F, it is concluded that the methanol molecules are distributed around the hydrophobic backbones with their methyl groups in contact with fluorine atoms and hydroxyl groups pointing to the hydrophilic subphase. While the water molecules and hydronium cations are distributed around the hydrophilic sulfonate anion groups with their hydrogen atoms in contact with the sulfonate oxygen atoms via hydrogen bonds (Figure 7c). We also generated the nearest distance distribution functions from several other history files recorded during molecular dynamics simulations starting from different initial configurations, and no significant difference was found. Therefore, we concluded that these nearest distance distribution functions do represent the really distribution of methanol, water, and hydronium in the hydrated PFSA.

3.2. The Hydration of Methanol and the Protonation of Hydrated Methanol Clusters. In the previous section, the hydrogen bond network in hydrated PFSA is studied using MD simulations. In this section, we will study the hydrogen bonding characteristics, especially the hydrogen bonding competition

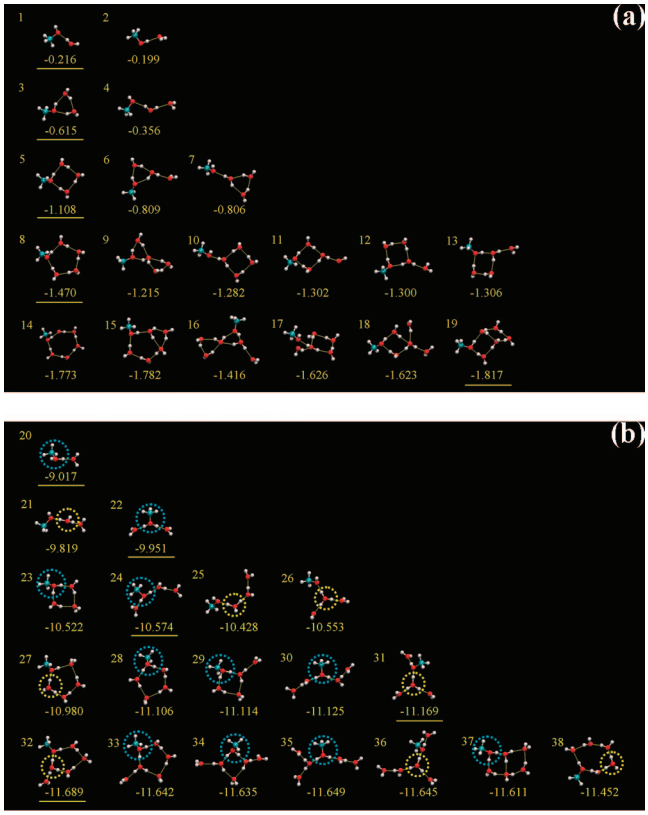

Figure 8. Typical stable conformations of (a) the hydrated methanol clusters $(CH_3OH)(H_2O)_n$ ($n = 1\sim5$); and (b) their corresponding protonated moieties $H^+(CH_3OH)(H_2O)_n$ optimized at the MP2/6-31++G (d, p) level of theory. The corresponding binding energy (eV) is reported below each conformation, and a binding energy underscored corresponds to the most stable conformation. The blue (or yellow) dotted cycles depict where the extra proton locates, blue for $CH_3OH_2^+$, yellow for H_3O^+.

between a methanol molecule and a water molecule of hydrated methanol clusters ($(CH_3OH)(H_2O)_n$, $n = 0\sim5$), as well as their corresponding protonated moieties ($H^+(CH_3OH)(H_2O)_n$, $n = 0\sim5$) using ab initio calculations. These characteristics are important to the understanding of proton transport and electroosmotic drag of the neutral molecules. All the geometrical optimizations are conducted at theory level of MP2/6-31++G(d, p) and are proved to be local minimum by a frequency calculation as implemented in Gaussian 03 program.[41] All the calculated energies are corrected with the zero-point energy.

All the optimizations are carried out from several initial conformations of neutral hydrated methanol clusters, as well as their corresponding protonated counterparts, including the linear conformations, the cyclic conformations, and branched cyclic conformation.[37,42−45] Some of the typical optimized conformations are shown in Figure 8, and their geometrical characteristics are summarized below. For description clarity, an oxygen atom in water will be labeled as hydrogen acceptor A-OW (or hydrogen donor D-OW) if the water molecule accepts a hydrogen atom (or donates a hydrogen atom) while forming hydrogen bonds. The extra hydrogen atom will be labeled as H^+ for the protonated clusters.

3.2.1. H_2O, CH_3OH, $H^+(H_2O)$, and $H^+(CH_3OH)$. The optimized bond length and bond angle for these four moieties are as follows. H_2O: H−O 0.963 Å, H−O−H 105.3°. CH_3OH: C−O 1.429 Å, O−H 0.964 Å, C−H 1.090 Å (mean value), C−O−H 108.5°. $H^+(H_2O)$: O−H 0.980 Å, H−O−H 112.5°. $H^+(CH_3OH)$: C−O 1.517 Å, O−H 0.978 Å, C−O−H 114.4°. Our calculated bond lengths and angles are in good agreement with experimental bond length 0.958 Å, and bond angle 104.5° for water; bond length C−O 1.425 Å, O−H 0.945 Å, C−O−H bond angle 108.5° for methanol.[46]

3.2.2. $(CH_3OH)(H_2O)$ and $H^+(CH_3OH)(H_2O)$. For the neutral cluster, there are two stable conformations (**1** and **2**), and **1** where methanol accepts a hydrogen in hydrogen bonding is slightly more stable than **2** where methanol donates a hydrogen in hydrogen bonding. For **1**, the calculated OM−(D−OW) distance is 2.856 Å, and OM−HW−(D−OW) is 170.3°. For **2**, the OM−(A−OW) is 2.909 Å, and the OM−HW−(A−OW) is 180.0°. For the protonated moiety, only one stable conformation **20** is obtained, and the extra proton closes to the methanol molecule forming a $CH_3OH_2^+$−H_2O conformation. The OM-H^+ distance is 1.058 Å and the OW−H^+ distance is 1.398 Å. These values close to other calculated values of 1.06 and 1.43 Å based on B3LYP/6-31+G* level of theory.[37] And the hydrogen bond OM−(H^+−OW) distance is 2.454 Å, and the OM−H^+−OW angle is 174.6°.

3.2.3. $(CH_3OH)(H_2O)_2$ and $H^+(CH_3OH)(H_2O)_2$. The neutral cluster forms one cyclic conformation **3** and one linear conformation **4**. The cyclic conformation where three hydrogen bonds are formed is 0.259 eV lower in energy than the linear conformation where only two hydrogen bonds are formed. In the cyclic conformation **3**, methanol acts both as hydrogen acceptor and hydrogen donor with OM−(D−OW) distance of 2.782 Å, and OM−(A−OW) distance of 2.804 Å. For the protonated cluster, a linear conformation **21** and a starlike conformation **22** are formed, and the starlike conformation **22** is slightly more stable than the linear conformation **21**. The starlike conformation **22** has symmetry with a protonated methanol $CH_3OH_2^+$ located in the center; both OM−HM bond lengths are 1.018 Å (same as calculated value in literatures[47]). Both OM−(H^+−OW) distances (at 2.533 Å) are within distance of strong hydrogen bonding.

3.2.4. $(CH_3OH)(H_2O)_3$ and $H^+(CH_3OH)(H_2O)_3$. Many stable conformations are obtained for these moieties, some of the typical conformations are shown in Figure 8. The neutral clusters tend to form cyclic conformation or branched cyclic conformations, and the closed cyclic conformation **5** is the most stable conformation. The hydrogen bonds formed in the branched cyclic conformations **6** and **7** are distorted compared to **5**. For the protonated cluster, the most stable conformation is the starlike conformation **24** where the extra proton is taken by the methanol forming a $CH_3OH_2^+$ moiety. The two OM−H bonds in 24 are 1.059 and 1.006 Å, similar to the average distance of 1.033 Å reported by Masamura calculated at theory level of MP2/6-31+G(d, p).[47] The other stable conformations include another starlike conformation **26,** where the extra proton is taken by the water molecule forming a H_3O^+ moiety, the cyclic conformation **23**, and the linear conformation **25**.

3.2.5. $(CH_3OH)(H_2O)_4$ and $H^+(CH_3OH)(H_2O)_4$. All the typical neutral conformations are cyclic or branched cyclic to form as many hydrogen bonds as possible. The most stable conformation is **8**, where a big closed cycle is formed. On the other hand, the protonated clusters could form both cyclic and acyclic conformations **27**∼**31**. Also, the acyclic starlike conformation **31** is the most stable one; its extra proton is shared between the methanol molecule and a water molecule. The OM−H^+ distance is 1.297 Å slightly longer than the OW−H^+ distance of 1.111 Å.

3.2.6. $(CH_3OH)(H_2O)_5$ and $H^+(CH_3OH)(H_2O)_5$. The neutral clusters are likely to form monocyclic, bicyclic, or branched cyclic conformations, and the bicyclic conformation **19** is

TABLE 2: Total Energies (TE), Hydration Energies (HE), Average Hydration Energies (AHE), and Marginal Hydration Energies (MHE) of Hydrated Methanol Molecules, and Their Corresponding Protonation Energies (PE) and Marginal Hydration Energies of Protonated Moieties (MPHE) Calculated at Theory Level of MP2/6-31++G(d, p)[a]

clusters	TE	HE	AHE	MHE	PE	MPHE
H_2O	−76.21175				−164.21	
CH_3OH	−115.34129				−179.75	
$(CH_3OH)(H_2O)$	−191.56099	−4.99	−4.99	−4.99	−202.93	
$(CH_3OH)(H_2O)_2$	−267.78738	−14.18	−7.09	−9.19	−215.15	−21.45
$(CH_3OH)(H_2O)_3$	−344.01727	−25.56	−8.52	−11.38	−218.15	−14.30
$(CH_3OH)(H_2O)_4$	−420.24233	−33.91	−8.48	−8.35	−223.68	−13.84
$(CH_3OH)(H_2O)_5$	−496.46680	−41.89	−10.47	−7.98	−227.60	−11.99

[a] Unit: Hartree for total energy; kcal/mol for various binding energies.

slightly more stable than the monocyclic conformation **14** or the bicyclic conformation **15**. The other branched bicyclic conformation **16** and branched monocyclic conformation **17** and **18** are more unstable. For the protonated clusters, the branched cyclic conformation **32** is the most stable one, and its extra proton is shared by the methanol molecule with a water molecule. The OW−H^+ distance of 1.111 Å is slightly shorter than the OM−H^+ distance of 1.302 Å.

In summary, there are two tendencies for the neutral clusters: cyclic conformations are favored since more hydrogen bonds are formed in the cyclic conformations than in the acyclic conformations, and the methanol molecule is more likely to occupy in a cyclic position instead of a branched position. For the protonated clusters, it is more likely to form starlike conformation where the proton is shared by the methanol molecule with a water molecule. If the cluster $H^+(CH_3OH)(H_2O)_n$ is small with $n = 1$, 2, or 3, the extra proton closes to the methanol forming a $CH_3OH_2^+$ cation. The OM−H^+ distances are 1.058, 1.018 and 1.059 Å, and OW−H^+ distances are 1.398, 1.517 and 1.389 Å, for $n = 1$, 2, or 3, respectively. If the cluster is large with $n = 4$ or 5, the extra proton closes to the water molecule forming a H_3O^+ cation. The OM−H^+ distance is 1.300 Å, and the OW−H^+ distance is about 1.111 Å. These results are in good accordance with the conclusion that methanol is basicity in gas (corresponding to a small cluster) and acidity in liquid (corresponding to a large cluster).[37] Therefore, it is concluded that the proton will be pulled from methanol to water as the content of water increases, in agreement with Kebarle's results[43] and our MD results.

The total energies, hydration energies, and protonation energies of hydrated methanol clusters $(CH_3OH)(H_2O)_n$ and their corresponding protonated moieties $H^+(CH_3OH)(H_2O)_n$ are summarized in Table 2. The methanol hydration energies (HE) are calculated as energy difference of reaction

$$CH_3OH + nH_2O \rightarrow (CH_3OH)(H_2O)_n$$

The average hydration energy (AHE) is the overall hydration energy divided by the number of water molecules n. The marginal hydration energy (MHE) is the hydration energy of the last water molecule. The protonation energy (PE) of the hydrated methanol cluster is derived according to the reaction

$$H^+ + (CH_3OH)(H_2O)_n \rightarrow H^+(CH_3OH)(H_2O)_n$$

And the marginal hydration energy of protonated moiety (MPHE) is the energy difference of:

$$H^+(CH_3OH)(H_2O)_{n-1} + H_2O \rightarrow H^+(CH_3OH)(H_2O)_n$$

The calculated proton affinity energies for methanol and water molecules at −179.75 and −164.21 kcal/mol agree well with the experimental values at −181 and −165 kcal/mol.[48,49] From Table 2, it also shows that the average hydration energy increases as the water content increases, that is to say, the methanol hydration cluster becomes more and more stable as hydration level increases. On the other hand, the marginal hydration energy increases from −4.99 to −11.38 kcal/mol as n increases from 1 to 3, and then decreases to −8.35 and −7.98 kcal/mol as n further increases to 4 and 5. This agrees with our molecular dynamics simulation where a first shell coordination number of 2.47 is observed; any extra water molecules (the fourth one) will fill into the second hydration shell of methanol. The protonation energy of the hydrated methanol cluster increases monotonically with the increase of the cluster size (table 2), and our calculated marginal hydration energies of protonated moieties, −21.45, −14.30, −13.84, and −11.99 kcal/mol, are slightly larger than that of −19.7, −13.1, −11.9, and −10.9 kcal/mol calculated at B3LYP/6-31+G* level of theory.[37]

3.3. Water Electroosmotic Drag and Methanol Crossover. In experiments or real world fuel cells, the electric field applied to the electrolyte membrane is usually less than 0.1 V/μm.[5,7] Under such electric field, the average transport velocities for hydronium cations, water molecules, or methanol molecules are very low and cannot be accurately evaluated using the state-of-the-art molecular dynamics simulation technique. Therefore, it is necessary to apply much high electric field to achieve significant transport velocities in molecular dynamics simulation. On the other hand, strong electric field will unavoidably disturb the microstructure of the hydrated PFSA membrane, and thus affect the transport characteristics.

3.3.1. Microstructure of PFSA under Electric Field. In Figure 9, it shows the microstructures of the PFSA hydrated by the aqueous methanol solution under various electric fields of 0, 1, 2, 5 V/μm. Under weak electric field, no significant difference in the microstructure is observed (Figure 9a,b). As the electric field increases to 2 V/μm, slight distortion in the microstructure of PFSA backbone is observed; however, the "water-in-oil" structure is still kept (Figure 9c). If the electric field increases to 5 V/μm, the hydrophobic subphase is seriously distorted, and even the "water-in-oil" structure is destroyed (Figure 9d). In addition, the density slightly varies from 1.61 to 1.60 g/cm^3 as the electric field increases from 0 to 1 or 2 V/μm, but decreases to 1.46 g/cm^3 as the electric field increases to 5 V/μm. Therefore, we conclude that an electric field of 2 V/μm or below is suitable, while 5 V/μm is not suitable for the molecular dynamics simulation study of electroosmosis.

3.3.2. Diffusion of Hydronium Cations, Water Molecules, and Methanol Molecules. The diffusion coefficient is directly calculated by mean square displacements in MD simulation. The calculated diffusion coefficient for hydronium is 0.944 × 10^{-5} cm/s^2. The calculated diffusion coefficient for water is 2.37 × 10^{-5} cm/s^2, higher than experimental value ranging from 0.3 to 1.2 x10^{-5} cm/s^2 in PFSA membrane hydrated by aqueous methanol solution.[9,13,50] Considering that the diffusion coefficient for TIP3P water is about twice of the experimental value of pure water,[51] this discrepancy could be attributed to the force field model. However, the calculated diffusion coefficient for methanol (0.66 × 10^{-5} cm/s^2) shows good correspondence with experimental values or calculated values in literatures. For instance, Ren reported diffusion coefficients of 0.5 × 10^{-5} cm/s^2 for methanol and 1.0 × 10^{-5} cm/s^2 for water at 30 °C, and practically constant regardless of the methanol concentration

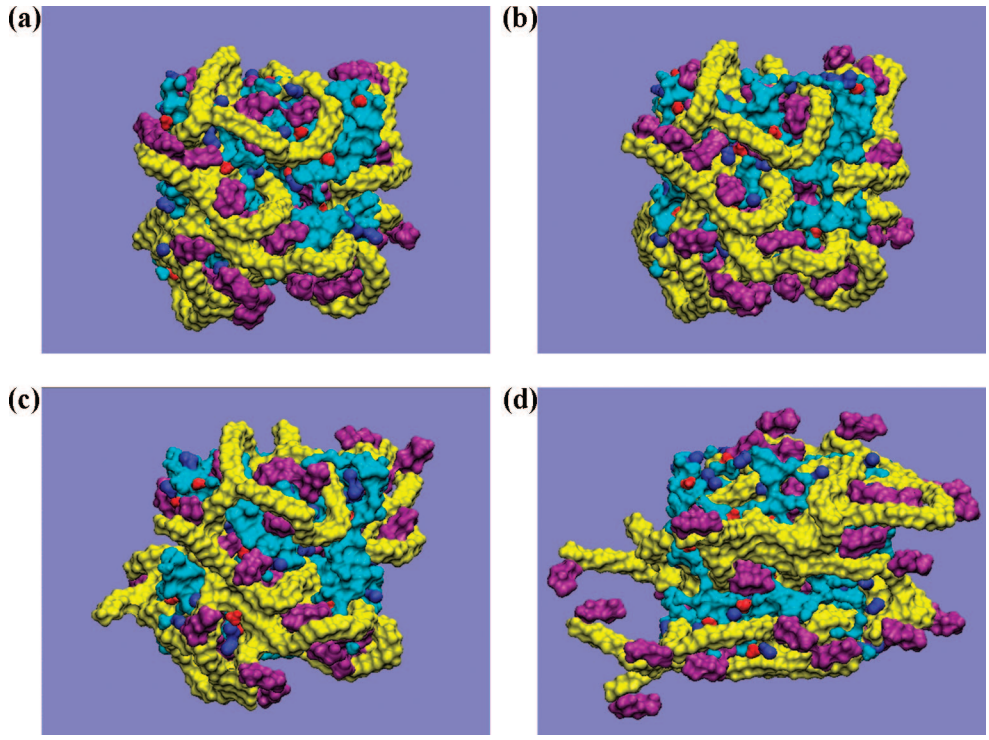

Figure 9. Snapshots of the simulated system with an electric field applied in the *x*-direction (from left to right) at (a) 0, (b) 1, (c) 2, and (d) 5 V/μm. Color codes: yellow for the PFSA backbone; purple for the PFSA side-chain; cyan for water; red for hydronium; and blue for methanol.

in range of 1∼8 mol/dm^3 in the hydrated NAFION 117 membrane using the pulsed field gradient spin−echo NMR method.[9] Meier reported a methanol diffusion coefficient of 0.44 and 0.66 × 10^{-5} cm/s^2 at 25 °C in NAFION 115 and 117 membrane hydrated by 0.3 mol/dm^3 aqueous methanol solution (hydration degree of 15∼35) using gas chromatography and found that the diffusion coefficient increases with the increase of temperature.[52] Cruickshank reported diffusion coefficient of 3.0 × 10^{-5} cm/s^2 for methanol in NAFION 117 membrane at 50 °C.[13] Schaffer determined a mean methanol diffusion coefficient of 0.25 × 10^{-5} cm/s^2 in NAFION 112, 0.24 × 10^{-5} cm/s^2 in NAFION 115, and 0.31 × 10^{-5} cm/s^2 in NAFION 117 at 23 °C using gas chromatography,[7] in which the water and methanol are in equimolar. The diffusion coefficient for methanol, reported by Hallinan et al. using time-resolved Fourier transform infrared-attenuated total reflectance (FTIR-ATR) spectroscopy, is between 0.220 and 0.584 × 10^{-5} cm/s^2, and that for water varies between 0.344 and 0.575 × 10^{-5} cm/s^2 as the methanol concentration in NAFION 117 varies from 1 and 16 mol/dm^3.[50] From these values, it could be concluded that our molecular dynamics evaluation of diffusion coefficient for methanol is in good correspondence with experimental results.

3.3.3. Transport Velocities for Hydronium Cations, Water Molecules, and Methanol Molecules. In a recent study, we introduced two methods to evaluate the transport velocities of hydronium and neutral water molecules in hydrated PFSA membrane with an electric field applied using molecular dynamics simulations.[17] In the first method, the transport velocities are evaluated as the ensemble averages of all the hydronium and water molecules in the simulated system. In the second method, the velocity distribution of the hydronium and water molecules are fitted to the peak-shifted Maxwell−Boltzmann velocity distribution functions in the direction of the electric field applied, and the transport velocities are approximated as the peak shifting velocities.

In this study, this procedure is applied to the evaluation of transport velocities for hydronium cations, water molecules, as well as methanol molecules. The equations are listed for convenience; the readers are referred to literature for the details.[17]

$$f(v) = 4\pi(m/2\pi k_B T)^{3/2} v^2 \exp(-mv^2/2k_B T) \quad (1)$$

$$f(v_\perp) = (m/2\pi k_B T_\perp)^{1/2} \exp(-mv_\perp^2/2k_B T_\perp) \quad (2)$$

$$f(v_\parallel) = (m/2\pi k_B T_{//})^{1/2} \exp(-m(v_\parallel - v_0)^2/2k_B T_\parallel) \quad (3)$$

where m is the molecular mass; k_B is the Boltzmann constant; $v_\perp$ or $v_\parallel$ denotes the velocity component perpendicular or parallel to the applied electric field; v is the molecular speed; v_0 is the peak shifting velocity corresponding to the transport velocity, and T, $T_\perp$, and $T_\parallel$ are parameters corresponding to the temperature.

The velocity distribution functions from molecular dynamics simulation under various applied electric fields, as well as their corresponding least-squares fits to the Maxwell−Boltzmann velocity distribution function are plotted in Figure 10. From these plots, it could found that all the speed distribution functions fit well to the Maxwell−Boltzmann speed distribution functions whether the moiety is charged or not and there is an electric field applied or not. Since a hydronium cation and a water molecule have similar molecular weight, their speed distribution functions are similar to each other. In direction perpendicular to the applied electric field, the velocity distribution functions fit well to the Maxwell−Boltzmann velocity distribution function independent of the strength of the electric field. In direction parallel to the applied electric field, the velocity distribution functions fit well to the peak-shifted Maxwell−Boltzmann velocity distribution function. Besides the similarity of all the velocity distribution functions, it could also be found that the peak of the velocity distribution in direction parallel to

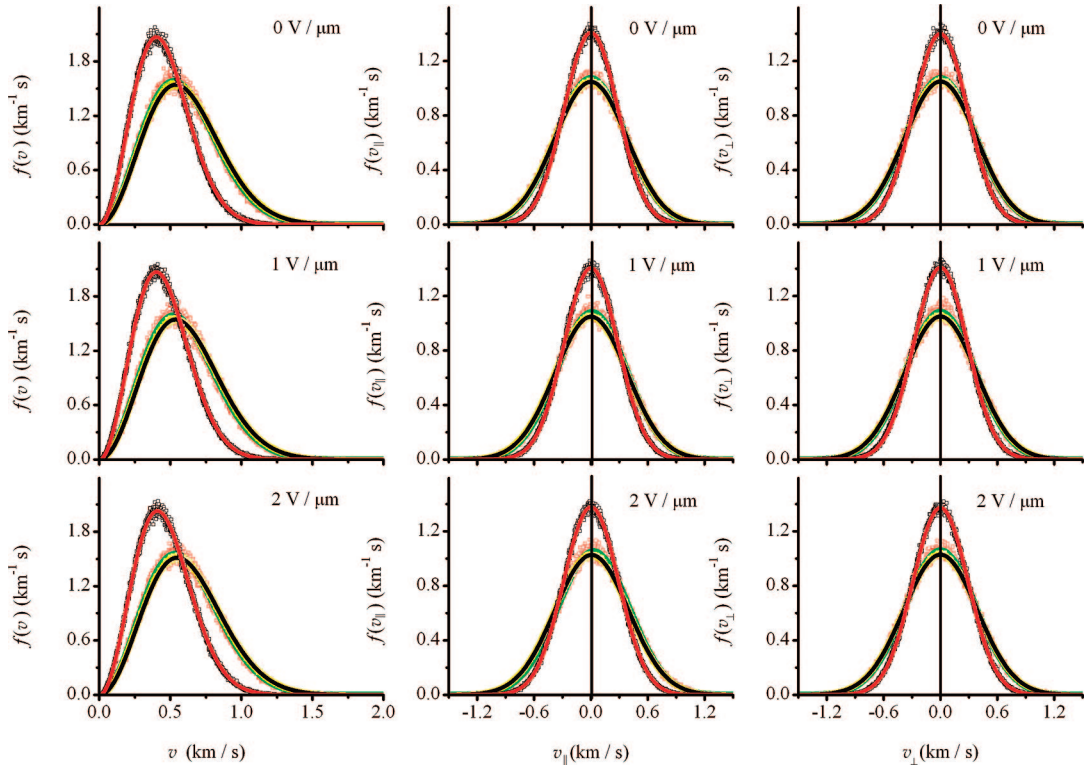

Figure 10. Speed and velocity distribution of the hydronium, water, and methanol in PFSA membrane hydrated by aqueous methanol solution with an electric field of 0, 1, and 2 V/μm applied in the x-direction. Left column, speed distribution function $f(v)$; middle column, velocity distribution function $f(v_{\parallel})$ of velocity component in direction parallel to the applied electric field; right column, velocity distribution function $f(v_{\perp})$ of velocity component in the direction perpendicular to the applied electric field. The red (or yellow, black) open squares represent data points of velocity distribution function of H_3O^+ (or H_2O, CH_3OH) evaluated from MD simulations; the green (or black, red) curves represent their corresponding least-squares fits to the Maxwell−Boltzmann velocity distribution functions (or the peak-shifted ones).

the electric field shifts away from zero and increases with the electric field.

From the velocity distribution functions in direction parallel to the electric field, the peak shifting velocities are summarized in Table 3. The peak shifting velocity v_0 for hydronium, water, and methanol are 9.96, 1.76, 0.36 m/s at 1 V/μm, and 27.28, 7.06, 1.10 m/s at 2 V/μm. In Table 3, it also lists the average transport velocities $\bar{v}_H$, $\bar{v}_W$, or $\bar{v}_M$ based on the ensemble averages of all the hydronium cations, water molecules, and methanol molecules in the simulated system. Comparing these two sets of data, it could be seen that average transport velocities and the peak shifting velocities for hydronium match well. However, the data for water and methanol molecules match only moderately due to the statistical errors.

3.3.4. The Electroosmotic Drag Coefficient and Methanol Crossover Coefficient. The transport flow of hydronium (water, or methanol) induced by the electric field without any other mechanisms could be evaluated as the product of the number concentration of hydronium (water, or methanol) and their peak shifting velocities

$$J_H = (n_H/V)v_{H,0} \quad (4)$$

$$J_W = (n_W/V)v_{W,0} \quad (5)$$

$$J_M = (n_M/V)v_{M,0} \quad (6)$$

where V is the volume of the simulated cell, n_H (n_W, or n_M) is the number of hydronium cations (water, or methanol molecules), and $v_{H,0}$ ($v_{W,0}$, or $v_{M,0}$) is the peak shifting velocity corresponding to the average transport velocity $\bar{v}_H$ ($\bar{v}_W$, or $\bar{v}_M$). From these transport flows, the electroosmotic drag coefficient of water or the methanol, or the number of water (or methanol) molecules transported accompanied with the transport of each hydronium, is calculated as

$$K_{drag}^{W} = (J_W + J_H)/J_H \quad (7)$$

$$K_{drag}^{M} = J_M/J_H \quad (8)$$

Two sets of electroosmotic drag coefficients of water and methanol, one calculated from the ensemble average velocities and the other calculated from the peak shifting velocities, are listed in Table 3. On the basis of the ensemble average velocities, the calculated electroosmotic drag coefficients are 5.32 (or 0.16) and 5.53 (or 0.14) for water (or methanol) at electric field strength of 1 V/μm and 2 V/μm, respectively. These values are slightly higher than those calculated from the peak shifting velocities, where the electroosmotic drag coefficients are 4.00 (or 0.07) and 5.32 (or 0.08) for water (or methanol) at 1 and 2 V/μm (the relative difference for methanol is larger owing to its small absolute electroosmotic drag coefficient).

4. Discussions and Conclusions

Although it is well accepted that the water and methanol transport in hydrated PFSA membrane could be described in terms of electroosmotic drag, diffusion, and convection,[8,17,53−55] molecular level description of their transport is still under development. In view of complexation, a bare proton must

TABLE 3: The Peak Shifting Velocities v_0, Average Transport Velocities $\bar{v}$ for Hydronium Cations, Water Molecules, and Methanol Molecules under Various Electric Fields E[a]

	Ensemble average velocities						Peak shifting velocities				
E	ρ	$\bar{v}_H$	$\bar{v}_W$	$\bar{v}_M$	K^W_{drag}	K^M_{drag}	$v_{H,0}$	$v_{W,0}$	$v_{M,0}$	K^W_{drag}	K^M_{drag}
0	1.61	0.00	0.00	0.00			0.00	0.00	0.00		
1	1.61	10.91	2.77	0.90	5.32	0.16	9.96	1.76	0.36	4.00	0.07
2	1.60	29.34	7.81	2.07	5.53	0.14	27.78	7.06	1.10	5.32	0.08

[a] Unit for E, V/μm; for v, m/s; for ρ, g/cm^3.

complex with other molecules in hydrated PFSA. For example, a bare proton could combine a few water molecules forming hydronium $H^+(H_2O)$, Zundel cation $H^+(H_2O)_2$, Eigen cation $H^+(H_2O)_4$, or combine a methanol molecule forming $H^+(CH_3OH)$, or even combine both water and methanol molecules forming $H^+(CH_3OH)(H_2O)$. As a proton transports under an applied electric field, the coordinated neutral water molecules or methanol molecules will also transport. This is the so-called vehicle mechanism or association mechanism.[8,17] Therefore, the electroosmotic drag coefficient could be evaluated as the average coordination number of water molecules or methanol molecules. As a matter of fact, the neutral water (or methanol) molecules in vicinity of a complex cation will also gain momentum transferred from the complex cations during their collision, thus these molecules will also transport under an applied electric field; this is the so-called momentum transfer mechanism.[17] By combination of the association mechanism and the momentum transfer mechanism, it could be concluded that the electroosmotic drag coefficient will be greater than the average coordination number. What makes the electroosmosis more complicated is proton hopping transport, or the Grotthus mechanism. When a proton hops between water (or methanol) molecules, no neutral water (or methanol) molecule was supposed to accompany with the proton.[8] Recently, we proposed a new mechanism for the electroosmosis based on momentum transport between a bare proton and a water molecule during the hopping of the proton, and concluded that the proton hopping will also contribute to the electroosmosis.[17] Suppose that J_H(veh) or J_H(hop) (J_W(veh) or J_W(hop); J_M(veh) or J_M(hop)) is proton (water; methanol) transport flow contributed exclusive by vehicle mechanism or hopping mechanism; then eqs 7 and 8 should be rewritten as

$$K^W_{drag} = \frac{J_W(\text{veh}) + J_W(\text{hop}) + J_H(\text{veh})}{J_H(\text{veh}) + J_H(\text{hop})} \quad (9)$$

$$K^M_{drag} = \frac{J_M(\text{veh}) + J_M(\text{hop})}{J_H(\text{veh}) + J_H(\text{hop})} \quad (10)$$

Since the vehicle mechanism contributes about 22% of the overall proton transport in hydrated NAFION membrane,[56] the hopping flow is 3.54 times that of the vehicle flow, or J_H(hop) = 3.54 J_H(veh). By applying the transport velocities in Table 3 to eq 9, we recalculate the electroosmotic drag coefficient for water at 0.88∼1.22 if it is assumed that J_W(hop) = 0, or at 2.23∼2.99 if it is assumed that J_W(hop) = J_W(veh).[17] As most of the experimental electroosmotic drag coefficients in literature are reported in range of 2.0∼3.0,[57−59] it is reasonable to hypothesize that hopping mechanism contributes similar transport for the neutral water molecules as the vehicle mechanism contributes.

Our molecular dynamics simulations show that the electroosmotic drag coefficient for methanol is in range of 0.07 to 0.16, much lower than that of water at 4.00 to 5.53. The electroosmotic drag coefficient for methanol will be adjusted to 0.65 to 1.48 if it is assumed that the concentration for methanol is the same as that of water. If it is also assumed that J_M(hop) = J_M(veh), the electroosmotic drag coefficients for methanol calculated using eq 10 will be in range of 0.29∼0.65. In their experiment, Tschinder et al. reported that the electroosmotic drag coefficients for methanol are lower than that for water if the concentration of methanol is below 40 vol %; however, it is almost the same if the concentration of methanol is above 40 vol%.[8] These experimental results do not conflict with our calculations

The low electroosmotic drag coefficient for methanol could be explained by the distribution of methanol molecules in the hydrated PFSA membrane. For example, Tschinder et al. argued that the stronger interaction between methanol and the PFSA polymer leads to the lower electroosmotic drag coefficient at lower temperatures.[8] In our simulation, it is concluded that methanol molecules are more likely to distribute in the vicinity of the hydrophobic backbones of PFSA with their methyl groups in direct contact with the fluorine atoms and hydroxyl groups in contact with the hydrophilic subphase. Therefore, the electroosmotic drag force on methanol molecules will be hindered by attraction from PFSA backbones.

Furthermore, our first principle calculations show that the proton prefers to form hydronium instead of $H^+(CH_3OH)$ as more water molecules are included to the protonated methanol clusters. That is to say, the $H^+(CH_3OH)$ is not a favored moiety in the hydrated PFSA membrane where enough water molecules exist in the neighborhood of every methanol molecule. Since the vehicle mechanism is directly related to the formation of complex cations, an unfavored $H^+(CH_3OH)$ will evidently cause the hindrance of electroosmotic drag of methanol. Therefore, we can conclude that both the vehicle mechanism and the hopping mechanism will bypass the electroosmotic drag of methanol at low concentration, and the major contribution of electroosmotic drag comes from the collision mechanism, which transfers momentum from hydronium.

Acknowledgment. The authors acknowledge the support from the Pujiang project of Shanghai Science and Technology Committee (No. 07PJ14044), the Department of Education of Shanghai and the Shanghai Leading Academic Discipline Project (No. J50101), and the National Science Foundation of China (No. 20873081). Part of the calculations were supported by "SEC E-Institute: Shanghai High Institutions Grid" project.

References and Notes

(1) Cremers, C.; Scholz, M.; Seliger, W.; Racz, A.; Knechtel, W.; Rittmayr, J.; Grafwallner, F.; Peller, H.; Stimming, U. Developments for improved direct methanol fuel cell stacks for portable power. *Fuel Cells* **2007**, *7* (1), 21–31.

(2) Icardi, U. A.; Specchia, S.; Fontana, G. J. R.; Saracco, G.; Specchia, V. Compact direct methanol fuel cells for portable application. *J. Power Sources* **2008**, *176* (2), 460–467.

(3) Höhlein, B.; Biedermann, P.; Grube, T.; Menzer, R. Fuel cell power trains for road traffic. *J. Power Sources* **1999**, *84* (2), 203–213.

(4) Baldauf, M.; Preidel, W. Status of the development of a direct methanol fuel cell. *J. Power Sources* **1999**, *84* (2), 161–166.

(5) Paik, Y.; Kim, S.-S.; Han, O. H. Methanol behavior in direct methanol fuel cells. *Angew. Chem., Int. Ed.* **2008**, *47* (1), 94–96.

(6) Han, J.; Liu, H. Real time measurements of methanol crossover in a DMFC. *J. Power Sources* **2007**, *164* (1), 166–173.

(7) Schaffer, T.; Tschinder, T.; Hacker, V.; Besenhard, J. O. Determination of methanol diffusion and electroosmotic drag coefficients in proton-exchange-membranes for DMFC. *J. Power Sources* **2006**, *153* (2), 210–216.

(8) Tschinder, T.; Schaffer, T.; Fraser, S. D.; Hacker, V. Electro-osmotic drag of methanol in proton exchange membranes. *J. Appl. Electrochem.* **2007**, *37* (6), 711–716.

(9) Ren, X.; Springer, T. E.; Zawodzinski, T. A.; Gottesfeld, S. Methanol transport through NAFION membranes: Electro-osmotic drag effects on potential step measurements. *J. Electrochem. Soc.* **2000**, *147* (2), 466–474.

(10) Kallio, T.; Kisko, K.; Kontturi, K.; Serimaa, R.; Sundholm, F.; Sundholm, G. Relationship between methanol permeability and structure of different radiation-grafted membranes. *Fuel Cells* **2004**, *4* (4), 328–336.

(11) Ramya, K.; Dhathathreyan, K. S. Methanol crossover studies on heat-treated NAFION membranes. *J. Membr. Sci.* **2008**, *311* (1−2), 121–127.

(12) Aricò, A. S.; Baglio, V.; Antonucci, V.; Nicotera, I.; Oliviero, C.; Coppola, L.; Antonucci, P. L. An NMR and SAXS investigation of DMFC composite recast NAFION membranes containing ceramic fillers. *J. Membr. Sci.* **2006**, *270* (1−2), 221–227.

(13) Cruickshank, J.; Scott, K. The degree and effect of methanol crossover in the direct methanol fuel cell. *J. Power Sources* **1998**, *70* (1), 40–47.

(14) Jeng, K. T.; Chen, C. W. Modeling and simulation of a direct methanol fuel cell anode. *J. Power Sources* **2002**, *112* (2), 367–375.

(15) Scott, K.; Taama, W.; Cruickshank, J. Performance of a direct methanol fuel cell. *J. Appl. Electrochem.* **1998**, *28* (3), 289–297.

(16) Schultz, T.; Sundmacher, K. Mass, charge and energy transport phenomena in a polymer electrolyte membrane (PEM) used in a direct methanol fuel cell (DMFC): Modelling and experimental validation of fluxes. *J. Membr. Sci.* **2006**, *276* (1−2), 272–285.

(17) Yan, L. M.; Ji, X. B.; Lu, W. C. Molecular dynamics simulations of electroosmosis in perfluorosulfonic acid polymer. *J. Phys. Chem. B* **2008**, *112* (18), 5602–5610.

(18) Jorgensen, W. L.; Maxwell, D. S.; Tirado-Rives, J. Development and testing of the OPLS all-atom force field on conformational energetics and properties of organic liquids. *J. Am. Chem. Soc.* **1996**, *118* (45), 11225–11236.

(19) Yan, L. M.; Zhu, S. H.; Ji, X. B.; Lu, W. C. Proton hopping in phosphoric acid solvated NAFION membrane: A molecular simulation study. *J. Phys. Chem. B* **2007**, *111* (23), 6357–6363.

(20) Sun, W.; Chen, Z.; Huang, S.-Y. Molecular dynamics simulation of liquid methanol under the influence of an external electric field. *Fluid Phase Equilib.* **2005**, *238* (1), 20–25.

(21) Urata, S.; Irisawa, J.; Takada, A. Molecular dynamics simulation of swollen membrane of perfluorinated ionomer. *J. Phys. Chem. B* **2005**, *109* (9), 4269–4278.

(22) Jorgensen, W. L.; Chandrasekhar, J.; Madura, J. D.; Impey, R. W.; Klein, M. L. Comparison of simple potential functions for simulating liquid water. *J. Chem. Phys.* **1983**, *79* (2), 926–935.

(23) Nosé, S. A molecular-dynamics method for simulations in the canonical ensemble. *Mol. Phys.* **1984**, *52* (2), 255–268.

(24) Smith W.; Leslie M.; Forester T. R. *Computer code DL_POLY_2.14*; CCLRC, Daresbury Laboratory: Daresbury, England, 2003.

(25) Verlet, L. Computer "experiments" on classical fluids. I. Thermodynamical properties of Lennard-Jones molecules. *Phys. Rev.* **1967**, *159* (1), 98–103.

(26) Hockney, R. W. Potential calculation and some applications. *Methods Comput. Phys.* **1970**, *9*, 135–211.

(27) Paddison, S. J. Proton conduction mechanisms at low degrees of hydration in sulfonic acid-based polymer electrolyte membranes. *Annu. Rev. Mater. Res.* **2003**, *33*, 289–319.

(28) Gierke, T. D.; Munn, G. E.; Wilson, F. C. The morphology in NAFION perfluorinated membrane products, as determined by wide- and small-angle x-ray studies. *J. Polym. Sci. Polym. Phys.* **1981**, *19* (11), 1687–1704.

(29) Vishnyakov, A.; Neimark, A. V. Molecular dynamics simulation of NAFION oligomer solvation in equimolar methanol-water mixture. *J. Phys. Chem. B* **2001**, *105* (32), 7830–7834.

(30) Morrone, J. A.; Tuckerman, M. E. *Ab initio* molecular dynamics study of proton mobility in liquid methanol. *J. Chem. Phys.* **2002**, *117* (9), 4403–4413.

(31) Zundel, G. Hydrogen bonds with large proton polarizability and proton transfer processes in electrochemistry and biology. *Adv. Chem. Phys.* **2000**, *111*, 1–217.

(32) Pomès, R.; Roux, B. Structure and dynamics of a proton wire: A theoretical study of H^+ translocation along the single-file water chain in the gramicidin A channel. *Biophys. J.* **1996**, *71* (1), 19–39.

(33) Park, Y. S.; Hatae, T.; Itoh, H.; Jang, M. Y.; Yamazaki, Y. High proton-conducting NAFION/calcium hydroxyphosphate composite membranes for fuel cells. *Electrochim. Acta* **2004**, *50* (2−3), 595–599.

(34) Banerjee, S.; Curtin, D. E. NAFION perfluorinated membranes in fuel cells. *J. Fluorine Chem.* **2004**, *125* (8), 1211–1216.

(35) Devanathan, R.; Venkatnathan, A.; Dupuis, M. Atomistic simulation of NAFION membrane: I. Effect of hydration on membrane nanostructure. *J. Phys. Chem. B* **2007**, *111* (28), 8069–8079.

(36) Hristov, I. H.; Paddison, S. J.; Paul, R. Molecular modeling of proton transport in the short-side-chain perfluorosulfonic acid ionomer. *J. Phys. Chem. B* **2008**, *112* (10), 2937–2949.

(37) Wu, C. C.; Jiang, J. C.; Boo, D. W.; Lin, S. H.; Lee, Y. T.; Chang, H. C. Behaviors of an excess proton in solute-containing water clusters: A case study of $H^+(CH_3OH)(H_2O)_{1-6}$. *J. Chem. Phys.* **2000**, *112* (1), 176–188.

(38) Li, S.; Tao, F.-M.; Gu, R. Theoretical study on the ionic dissociation of halosulfonic acids in small water clusters. *Chem. Phys. Lett.* **2006**, *426* (1−3), 1–7.

(39) Meijer, E. J.; Sprik, M. *Ab initio* molecular dynamics study of the reaction of water with formaldehyde in sulfuric acid solution. *J. Am. Chem. Soc.* **1998**, *120* (25), 6345–6355.

(40) Narten, A. H. Liquid Water: Atom pair correlation functions from neutron and x-ray diffraction. *J. Chem. Phys.* **1972**, *56* (11), 5681–5687.

(41) Frisch, M. J.; Trucks, G. W.; Schlegel, H. B.; Scuseria, G. E.; Robb, M. A.; Cheeseman, J. R.; Montgomery, J. A.; Vreven, T., Jr; Kudin, K. N.; Burant, J. C.; Millam, J. M.; Iyengar, S. S.; Tomasi, J.; Barone, V.; Mennucci, B.; Cossi, M.; Scalmani, G.; Rega, N.; Petersson, G. A.; Nakatsuji, H.; Hada, M.; Ehara, M.; Toyota, K.; Fukuda, R.; Hasegawa, J.; Ishida, M.; Nakajima, T.; Honda, Y.; Kitao, O.; Nakai, H.; Klene, M.; Li, X.; Knox, J. E.; Hratchian, H. P.; Cross, J. B.; Adamo, C.; Jaramillo, J.; Gomperts, R.; Stratmann, R. E.; Yazyev, O.; Austin, A. J.; Cammi, R.; Pomelli, C.; Ochterski, J. W.; Ayala, P. Y.; Morokuma, K.; Voth, G. A.; Salvador, P.; Dannenberg, J. J.; Zakrzewski, V. G.; Dapprich, S.; Daniels, A. D.; Strain, M. C.; Farkas, O.; Malick, D. K.; Rabuck, A. D.; Raghavachari, K.; Foresman, J. B.; Ortiz, J. V.; Cui, Q.; Baboul, A. G.; Clifford, S.; Cioslowski, J.; Stefanov, B. B.; Liu, G.; Liashenko, A.; Piskorz, P.; Komaromi, I.; Martin, R. L.; Fox, D. J.; Keith, T.; Al-Laham, M. A.; Peng, C. Y.; Nanayakkara, A.; Challacombe, M.; Gill, P. M. W.; Johnson, B.; Chen, W.; Wong, M. W.; Gonzalez, C.; Pople, J. A. *Gaussian 03*, Revision C.2; Gaussian, Inc.: Wallingford, CT, 2004.

(42) Wu, C. C.; Chaudhuri, C.; Jiang, J. C.; Lee, Y. T.; Chang, H. C. Structural isomerism and competitive proton solvation between methanol and water in $H^+(CH_3OH)_m(H_2O)_n$, $m + n = 4$. *J. Phys. Chem. A* **2004**, *108* (15), 2859–2866.

(43) Kebarle, P.; Haynes, R. M.; Collins, J. G. Competitive solvation of the hydrogen ion by water and methanol molecules studied in the gas phase. *J. Am. Chem. Soc.* **1967**, *89* (23), 5753–5757.

(44) Garvey, J. F.; Herron, W. J.; Vaidyanathan, G. Probing the structure and reactivity of hydrogen-bonded clusters of the type $(M)_n(H_2O)H^+$, via the observation of magic numbers. *Chem. Rev.* **1994**, *94* (7), 1999–2014.

(45) Furuhama, A.; Dupuis, M.; Hirao, K. Application of a kinetic energy partitioning scheme for *ab initio* molecular dynamics to reactions associated with ionization in water tetramers. *Phys. Chem. Chem. Phys.* **2008**, *10* (15), 2033–2042.

(46) Seo, Y.; Kim, Y.; Kim, Y. MC-QCISD calculations for proton affinities of molecules and geometries. *Chem. Phys. Lett.* **2001**, *340* (1−2), 186–193.

(47) Masamura, M. *Ab initio* molecular orbital study on the structures and energetics of $CH_3OH_2^+(H_2O)_n$ and $CH_3SH_2^+(H_2O)_n$ in the gas phase. *J. Comput. Chem.* **2001**, *22* (1), 125–131.

(48) Jursic, B. S. Complete basis set, Gaussian, and hybrid density functional theory evaluation of the proton affinities of water and ammonia. *J. Mol. Struct. (Theochem.)* **1999**, *490* (1−3), 1–6.

(49) Bouchoux, G.; Nadège, C. Intramolecular hydrogen migrations in ionized aliphatic alcohols. Barton type and related rearrangements. *Int. J. Mass Spectrom.* **2000**, *201* (1−3), 161–177.

(50) Hallinan, D. T. J.; Elabd, Y. A. Diffusion and sorption of methanol and water in NAFION using time-resolved Fourier transform infrared-attenuated total reflectance spectroscopy. *J. Phys. Chem. B* **2007**, *111* (46), 13221–13230.

(51) Guillot, B. A reappraisal of what we have learnt during three decades of computer simulations on water. *J. Mol. Liq.* **2002**, *101* (1−3), 219–260.

(52) Meier, F.; Kerres, J.; Eigenberger, G. Methanol diffusion in water swollen ionomer membranes for DMFC applications. *J. Membr. Sci.* **2004**, *241* (1), 137–141.

(53) Xu, C.; Zhao, T. S.; Yang, W. W. Modeling of water transport through the membrane electrode assembly for direct methanol fuel cells. *J. Power Sources* **2008**, *178* (1), 291–308.

(54) Rivin, D.; Meermeier, G.; Schneider, N. S.; Vishnyakov, A.; Neimark, A. V. Simultaneous transport of water and organic molecules through polyelectrolyte membranes. *J. Phys. Chem. B* **2004**, *108* (26), 8900–8909.

(55) Barragán, V. M.; Ruiz-Bauzá, C.; Villaluenga, J. P. G.; Seoane, B. Transport of methanol and water through NAFION membranes. *J. Power Sources* **2004**, *130* (1−2), 22–29.

(56) Kreuer, K.-D.; Rabenau, A.; Weppner, W. Vehicle mechanism, A new model for the interpretation of the conductivity of fast proton conductors. *Angew. Chem., Int. Ed. Engl.* **1982**, *21* (3), 208–209.

(57) Ise, M.; Kreuer, K. D.; Maier, J. Electroosmotic drag in polymer electrolyte membranes: An electrophoretic NMR study. *Solid State Ionics* **1999**, *125* (1−4), 213–223.

(58) Ren, X.; Gottesfeld, S. Electro-osmotic drag of water in poly(perfluorosulfonic acid) membranes. *J. Electrochem. Soc.* **2001**, *148* (1), A87−A93.

(59) Ren, X.; Henderson, W.; Gottesfeld, S. Electro-osmotic drag of water in ionomeric membranes. New measurements employing a direct methanol fuel cell. *J. Electrochem. Soc.* **1997**, *144* (9), L267−L270.

JP8066469